Why Galaxies Care About AGB Stars:
A Continuing Challenge through Cosmic Time
Proceedings IAU Symposium No. 343, 2019
F. Kerschbaum, M. Groenewegen & H. Olofsson, eds.

doi:10.1017/S174392131800724X

The mass-loss characteristics of AGB stars An observational view

Sofia Ramstedt

Division of Astronomy and Space Physics, Department of Physics and Astronomy,
Uppsala University
email: sofia.ramstedt@physics.uu.se

Abstract. The massive outflows of gas and dust which characterize giant stars on the Asymptotic Giant Branch (AGB), build cool circumstellar envelopes readily observed at infrared (IR) and sub-millimeter wavelengths. The observations will give the amount of matter lost by the star, the wind velocity (in the case of spectral line observations), and, when the spatial resolution is sufficient, the wind evolution over time. To gain detailed insight into the mass-loss process, we study the nearby (closer than 1 kpc) stars. Through these investigations we aim to determine the best constrained wind properties available. By combining this with theoretical results, mass-loss estimates for more distant sources can also be significantly improved. ALMA has opened up new opportunities to study the winds of AGB stars. The DEATHSTAR project (www.astro.uu.se/deathstar) has mapped the circumstellar CO emission from so far ∼50 nearby M- and C-type AGB stars. The data will initially be used to give a definitive mass-loss prescription for the sample sources, but the large-bandwidth observations opens for many different legacy projects. The current status and results are presented.

Keywords. AGB and post-AGB, circumstellar matter, mass-loss

1. Introduction

Molecular line emission in the sub-millimeter and millimeter regime is considered to be the most reliable indicator of the physical properties of circumstellar envelopes (CSEs) of AGB stars. Even so, the uncertainties of state-of-the-art mass-loss-rate estimates will reach as high as a factor of three (Ramstedt *et al.* 2008). As emphasized by recent high-spatial resolution observations (e.g., Guélin *et al.* 2018), an important factor is the impact of 3D effects such as asymmetries and clumpy structures in the outflows. Additional uncertainties are related to the thermodynamics of the CSEs and data calibration errors. Furthermore, this method has a limited reach due to the still restricted spatial resolution and signal-to-noise ratio that can be achieved in this long-wavelength regime, and therefore, methods used for more distant sources also have to be further developed. For sources beyond more than 1 kpc, the mass-loss-rate estimates are usually based on IR observations that probe the circumstellar dust emission, and an assumed gas-to-dust mass ratio. Recent theoretical results (e.g., Eriksson *et al.* 2014; Bladh *et al.* 2015; *this volume*; Nanni *et al.* 2018) show that the usually assumed gas-to-dust ratio of 200, and thereby the estimated mass-loss rates, could be significantly underestimated.

2. Methods to estimate mass-loss rates from single-pointing observations

2.1. *Observations of circumstellar envelopes*

The main constituent of AGB CSEs is cool gas, mainly in molecular form, with a gas-to-dust-mass ratio usually assumed to be of the order of 200. The most abundant

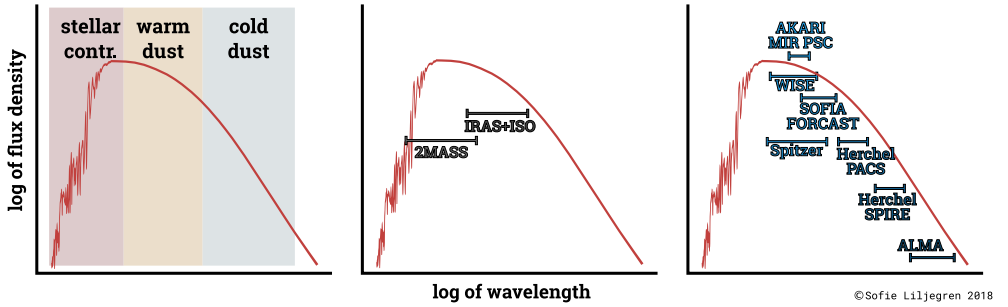

Figure 1. Left: Schematic overview of a typical SED (in log-scale) of a (carbon-rich) AGB star. Middle: Wavelength coverage of publicly available IR data before the turn of the century. Right: Wavelength coverage of recently observed and publicly available IR data. See text for references. Image credit: Sofie Liljegren.

molecule is H_2, but since it is not readily observable, CO rotational line emission is considered to be the most reliable probe for the physical conditions in CSEs. Single-pointing observations of low-J (<5) transitions have been collected for the AGB stars within a distance of about 1 kpc over the last several decades (see e.g., Teyssier *et al.* 2006; Ramstedt *et al.* 2009; De Beck *et al.* 2010, for recent examples). The Herschel/HIFI instrument also made higher-J transition line emission available for a relatively large fraction of the nearby sources (e.g., Justtanont *et al.* 2012; Danilovich *et al.* 2015b). The mass-loss-rate estimates based on these types of observations are representative of the average mass-loss rate over the time of the creation of the emitting region and are not necessarily a good measure of the current mass-loss rate from a star. With the Atacama Large Millimeter/submillimeter Array (ALMA) it has also for the first time been possible to resolve and detect CO line emission toward a few individual AGB stars in the Large Magellanic Cloud (LMC; Groenewegen *et al.* 2016).

The spectral energy distribution (SED) of a typical AGB star will show emission from a few tenths of a μm to some thousand μm and peak at around 1 μm. The dust emission will contribute significantly beyond $\sim$5 μm. Observations in this wavelength range require space-based facilities and several instruments have added to the available data base of IR observations of AGB stars in recent years (Fig. 1): AKARI (e.g., Ishihara *et al.* 2011), Spitzer (e.g., Meixner *et al.* 2006; Matsuura *et al.* 2013), WISE (e.g., Lian *et al.* 2014), Herschel PACS and SPIRE (Groenewegen *et al.* 2011), and SOFIA (e.g. Hankins *et al.* 2018). A comprehensive overview of the far-IR emission from nearby AGB stars is given in Cox *et al.* (2012) with images at 70 and 160 μm from Herschel/PACS. The authors focus on large-scale structure and wind-ISM interaction and classify the sources in four distinct categories (fermata, eyes, irregular, rings). Bow shocks are detected for 40% of the sources.

2.2. *Radiative transfer models of circumstellar envelopes*

Most estimates of mass-loss rates and other physical and chemical parameters are based on a standard description of the CSE: "The standard model" (Höfner & Olofsson 2018). In this model, the CSE is assumed to be homogeneous, spherical, and created by a constant stellar mass-loss rate. It is expanding at a constant velocity and in some calculations a thin inner acceleration region is included (e.g., Danilovich *et al.* 2015b). Micro-turbulent (of the order of 1.0 km s^{-1}) and local thermal contributions are added to the line broadening. The mass-loss rate is given by the conservation of mass: $\dot{M} = 4\pi r^2 v(r)\rho(r)$, where $v(r)$ is just the terminal expansion velocity, v_∞, if a constant expansion velocity is assumed.

https://doi.org/10.1017/S174392131800724X Published online by Cambridge University Press

The circumstellar temperature distribution is determined by different heating and cooling processes according to the energy-balance equation (e.g., Goldreich & Scoville 1976). The heating of the gas is predominantly due to collisions with the dust grains. The cooling is mainly due to the adiabatic expansion of the gas with significant contributions from line cooling from the most abundant radiating molecules, e.g., CO across the CSE, and H_2O and HCN in the inner CSE. The gas in low-mass-loss-rate CSEs is in most cases found to be warmer than the gas in high-mass-loss-rate CSEs. This is due to the more efficient line cooling, and less efficient heating at lower drift velocities between the gas and dust, in the high-mass-loss-rate CSEs.

The CO abundance distribution is commonly calculated using the model presented in Mamon *et al.* (1988). There is however growing evidence that this approach needs to be revised (Li *et al.* 2014; 2016; Groenewegen 2017; Saberi et al. *this volume*). Under typical CSE conditions it is sufficient to include the ground and first vibrational states and ∼40 rotational levels in the description of the CO molecule as found in the LAMBDA† data base (Schöier *et al.* 2005). The radiation from the central source is usually included in the form of a blackbody with the stellar effective temperature. In addition, thermal emission from the dust grains distributed across the CSE, as well as emission from the cosmic microwave background (mainly affecting the outer CSE) is included (see Höfner & Olofsson 2018, and references therein).

Observations of the broad continuum observations covering the SED can be modelled to estimate the dust optical depth. A dust-mass-loss-rate is then calculated through assumptions about the dust optical properties and the dust expansion velocity. The dust temperature distribution is determined by the balance between absorption and emission of radiation from the dust grains. The estimated mass-loss rate is more reliable, and averaged over a longer timescale, if the model is constrained using data covering the full breadth of the SED. An even higher accuracy is achieved if the continuum observations are complemented with some line measure to constrain the expansion velocity (e.g., OH maser emission lines), since the dust kinematics cannot be directly measured. Emission from the central source is usually included in the form of output from a hydrostatic stellar atmosphere model (e.g., MARCS; Gustafsson *et al.* 2008, or COMARCS; Aringer *et al.* 2009) when modelling the SED. For sources beyond ∼1 kpc, IR observations are essentially the only available probe that can be used to estimate mass-loss rates from AGB stars. Recent examples from the Local group are given in e.g., Gullieuszik *et al.* (2012) and Groenewegen & Sloan (2018).

3. Current results from CO line observations

AGB stars are divided into three main spectral types depending on the relative strength of molecular bands indicative of the C/O-ratio in their atmospheres: M-type stars (C/O < 1), S-type stars (C/O $\lesssim 1$), and C-type or carbon stars (C/O > 1). Mass-loss rates of nearby AGB stars from radiative transfer modelling of CO line observations are given in Schöier & Olofsson (2001; carbon stars), González-Delgado *et al.* (2003; M-type stars), and in Ramstedt *et al.* (2006; 2009; S-type and the summary of the full nearby sample). The three samples are essentially complete out to 500 pc. Mass-loss rates versus the terminal velocities (determined from the width of the CO lines taking other line broadening mechanisms into account) are shown in Fig. 2 together with the recent estimates for the LMC ([Fe/H]=-0.37 dex; open symbols) sources observed with ALMA (see above; Groenewegen *et al.* 2016). It is not straight-forward to compare wind properties at different metallicities, as it is not appropriate to directly compare CO-line-emission and

† `http://home.strw.leidenuniv.nl/~moldata/`

https://doi.org/10.1017/S174392131800724X Published online by Cambridge University Press

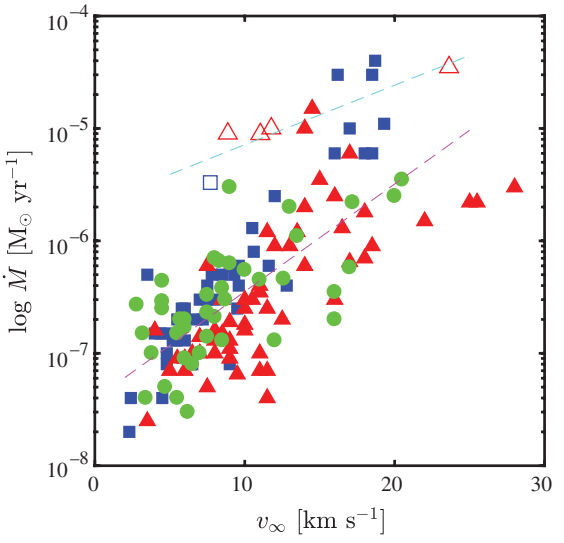

Figure 2. Mass-loss rates and wind velocities from CO line observations for carbon stars (red triangles), M-type stars (blue squares), and S-type stars (green dots). Filled symbols represent nearby, Galactic sources (Ramstedt *et al.* 2009, and references therein), and open symbols mark the recently observed LMC sources (Groenewegen *et al.* 2016). Basic linear fits to the LMC (dashed cyan) and nearby, Galactic (dashed magenta) samples are shown to guide the eye.

dust-continuum estimates, unless explicit care has been taken to calculate them consistently and therefore the comparison is made only for the mass-loss rates estimated using CO observations (for the LMC sources, using the relation given in Ramstedt *et al.* 2008). As seen in Fig. 2, the nearby Galactic sources of all three spectral/chemical types cover the same ranges in, and follow a similar correlation between, the wind properties. This suggests that the wind is driven by the same processes regardless of chemistry. However, as also seen in Fig. 2, it seems that the correlation between the wind parameters could be different at lower metallicity, as also suggested by Groenewegen *et al.* 2016, but this has to be confirmed by further CO observations of resolved LMC sources (or updated dust mass-loss-rate models for the nearby sources).

4. Overview from larger samples

It is clear that reliable mass-loss-rate estimates from larger samples of stars and from lower-metallicity sources are necessary to be able to determine the impact of the AGB stars on the galaxies they live in. The relation between the mass-loss rate of a star and it's basic stellar parameters in some sense hold the key to stellar evolution modelling and the derivation of the stellar yields from a theoretical perspective. There has therefore been attempts to derive empirical correlations between the mass-loss rates and stellar parameters (e.g., van Loon *et al.* 2005; Cummings *et al.* 2016) using different types of mass-loss-rate estimates. However, the outcome is inconclusive. The functional dependence of the mass-loss rate on the stellar luminosity (L) for instance ranges from almost linear for a sample of oxygen-rich giants in the LMC (from SED modelling; van Loon *et al.* 2005), to as steep as L^5 for a sample of nearby stars (from CO line modelling; Danilovich *et al.* 2015b). Another example is given by Riebel *et al.* (2012). Photometry observations (optical to mid-IR) of 30000 LMC stars are fitted using a large grid of dust radiative transfer models with varying stellar parameters and dust properties (GRAMS;

https://doi.org/10.1017/S174392131800724X Published online by Cambridge University Press

e.g., Sargent *et al.* 2011). In this work, no clear trend between the dust mass-loss rates and stellar luminosities is found. The discrepancies between the different results and methods show that there is still a lot of work that needs to be done to evaluate and improve the reliability of mass-loss-rate estimates, in particular for more distant sources. Some of the problems are likely due to that wind formation, and its evolution over time, gives rise to significant 3D effects.

5. Gas-to-dust mass ratios

Models of the dust continuum emission will give the dust density distribution and, with an assumption about the dust expansion velocity, the dust mass-loss rate (see continuity equation given above). To calculate the total mass-loss rate, the gas-to-dust mass ratio needs to be assumed. The standard value used in e.g. the widely spread public code DUSTY (Ivezic *et al.* 1999) is 200 (Groenewegen 2006; Groenewegen *et al.* 2007; 2009; Gullieuszik *et al.* 2012; Boyer *et al.* 2012; Srinivasan *et al.* 2006). Radiation-hydrodynamic wind models, including grain formation and growth where wind properties are calculated from first principles (Eriksson *et al.* 2014; Bladh *et al.* 2015; *this volume*), give a significantly higher value (of the order of 1000 and above). The same is found from recent estimates of the dust production rate at different metallicities based on stellar evolution models (e.g., Nanni *et al.* 2018). These model results need to be constrained by observations. Comparisons between consistent calculations of gas and dust mass-loss rates from observations give similar high values (Ramstedt *et al.* 2008), but they only exist for a small number of sources. A larger sample of observations would give stronger constraints to the theoretical results, however, this could mean that a large fraction of the mass-loss rates derived for more distant sources are significantly underestimated (by as much as a factor of 5-10). If so, this can have a large impact on stellar yield calculations and on investigations of the dust production across the Universe.

6. High-spatial resolution CO line observations

With earlier generations of submillimeter interferometers, it was possible to resolve the large-scale radial structure of the CSEs in some of the most nearby AGB stars (e.g., Castro-Carrizo *et al.* 2010). In recent years, the exceptional sensitivity and resolving power of ALMA has revolutionized the field by mapping CSEs of nearby AGB stars in remarkable detail (e.g., Maercker *et al.* 2012; Kim *et al.* 2017; Ramstedt *et al.* 2017; Bujarrabal *et al.* 2018), and by enabling studies of dynamical processes even on stellar scales (e.g., Vlemmings *et al.* 2018). The detailed images have opened up the possibility to directly track one of the most important aspects missing from our understanding of late stellar evolution; the evolution of the mass-loss rate and wind kinematics over time. New discoveries on the shaping of CSEs by a binary companion have been made, relevant in particular when studying the formation of planetary nebulae (Jones & Boffin 2017) and supernovae Type Ia (Maoz *et al.* 2014). Of course, the radiative transfer models needed to reproduce the three-dimensional images from interferometric observations require a higher level of complexity than the 1D models discussed above. The analysis of ALMA images has therefore in many cases consisted in comparing structures in the density distribution derived from hydrodynamic models directly with the images, however, some recent attempts at full 3D radiative transfer modelling also exist.

6.1. *Two recent examples: W Aql and π^1 Gru*

W Aql and π^1 Gru are two well-studied S-type AGB stars that are part of a small sample of binary AGB stars observed with ALMA. The sample (also including R Aqr and

https://doi.org/10.1017/S174392131800724X Published online by Cambridge University Press

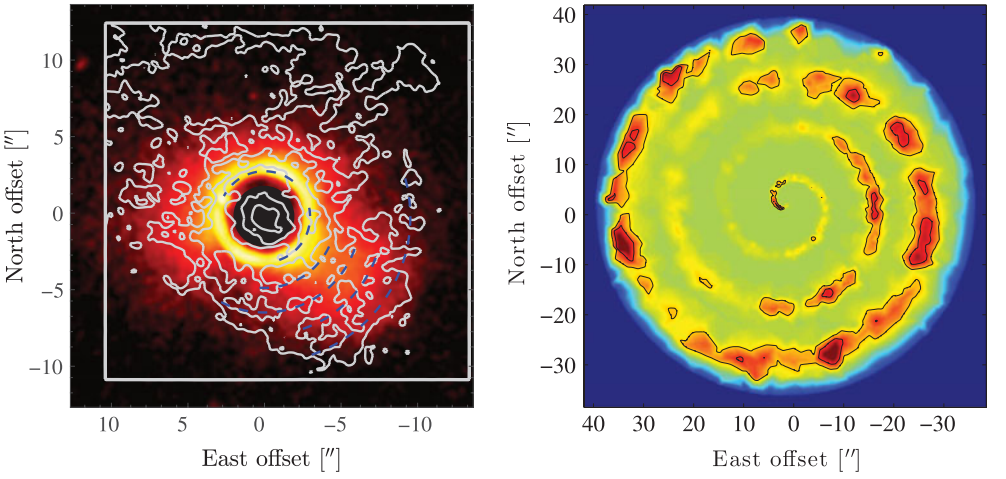

Figure 3. Left: The polarized scattered light emission from W Aql tracing the dust distribution overlayed with contours of the central-channel CO($J = 3 - 2$) emission from ALMA. The stars are covered by a coronograph and blue dashed lines are drawn to emphasize the arcs seen in the gas distribution. Right: Predicted CO($J = 3 - 2$) emission from a 3D radiative transfer calculation of a hydrodynamical wind-RLOF model of the system assuming an orbit eccentricity of e=0.2. See text for details and references.

Mira; Ramstedt *et al.* 2014; 2018) was selected so that the sources are observable from ALMA, have binary companions, and that some constraints on the binary orbit exists. The aim was to provide observational constraints for hydrodynamical models studying the interaction between the wind and a binary companion (wind-Roche-Lobe-OverFlow (wind-RLOF) models; Mohamed & Podsiadlowski 2012) by covering a range in binary separation and in wind velocity. With the data and analysis at hand, it becomes apparent that reproducing the CSEs of the sources is a too ambitious goal since the molecular gas distribution is affected by several effects that are not always accounted for in the models, i.e., wind from the companion (Mira; Ramstedt *et al.* 2014), radiation field of the companion (Mira, R Aqr; Ramstedt *et al.* 2018; Bujarrabal *et al.* 2018), additional companions (W Aql, π^1 Gru; Doan *et al.* 2017), and possible wind-variations over time (Mira, W Aql; Ramstedt *et al.* 2017).

Observations of the circumstellar dust and gas distributions around W Aql are shown in Fig. 3 (left). The binary pair was resolved by HST observations with a binary separation of 0.46" and the companion with a projected position southwest of the AGB star (Ramstedt *et al.* 2011; Danilovich *et al.* 2015a). The circumstellar dust distribution from observations of polarized scattered light is asymmetric with more material on the southwest side. ALMA observations of the CO($J = 3 - 2$) emission (Ramstedt *et al.* 2017) show the same southwest enhancement, but essentially the gas component is dominated by smooth, extended emission as would be expected from "the standard model". In addition, the velocity-resolved ALMA observations revealed a pattern of higher-density arcs across the southwest density enhancement. Figure 3 (right) show the predicted CO($J = 3 - 2$) emission from a 3D radiative transfer model (LIME; Brinch & Hogerheijde 2010) using the density and temperature distribution from a 3D SPH wind-RLOF model with the known parameters of the W Aql-system and an orbit eccentricity of $e = 0.2$. The distribution seen in the observations and the emission pattern predicted from the models are similar with enhanced arcs found on the west and southwest side of the binary pair. However, as seen in Fig. 3 the scales are different and the arc-separation is not the same in the two images. Closer investigation of the ALMA images showed an even weaker

https://doi.org/10.1017/S174392131800724X Published online by Cambridge University Press

additional arc-pattern with the same separation as predicted from the known companion. In conclusion, the system shows a circumstellar distribution very similar to that predicted from the model, however, in addition to that, smaller separation arcs are found with a creation timescale (∼200 yrs) which is inconsistent with any known process of the system. A possible explanations for the smaller-separation arcs could be 3D pulsation effects (Liljegren *et al.* 2017, *this volume*) or an additional, closer, previously unknown companion.

Out of the four binary sources observed as a sample with ALMA, π^1 Gru has the largest-separation companion (2.6" ≈ 400 AU at a distance of 395 pc). The circumstellar distribution, with a large, equatorial, slowly expanding ($v_\infty \approx 15\,\mathrm{km\,s^{-1}}$) torus and a higher-velocity ($v_\infty \approx 60\,\mathrm{km\,s^{-1}}$) bi-polar outflow, already early lead to the suggestion that a closer, undetected companion must be present (Sahai 1992). The combined CO line interferometry data of the system (CO($J = 2 - 1$) from SMA; Chiu *et al.* 2006, CO($J = 3 - 2$) from ALMA-ACA) is analysed in Doan *et al.* (2017). The new, high-resolution ALMA observations show arcs or a spiral density pattern across the torus very likely caused by the closer companion. The high-resolution data is analysed in detail in an upcoming paper by Doan et al..

6.2. *Outlook: The DEATHSTAR project*

The DEATHSTAR† (DEtermining Accurate mass-loss rates for THermally pulsing AGB STARs) project on ALMA is currently gathering observations of the CO $J = 2 - 1$ and $3 - 2$ emission from 67 nearby (closer than 1 kpc) M-, C- and S-type AGB stars using the Atacama Compact Array (ACA). The data will provide the necessary observational constraints needed for the radiative transfer models used to determine the physical parameters (mass-loss rate and temperature distribution) of the CSEs to not be dependent on the outdated photodissociation model by Mamon *et al.* (1988). Instead, the size of the emitting regions are measured directly.

So far, about 50 sources have been observed and the data have been delivered and reduced. For most of the sources, the interferometer recovers the main part of the flux measured in previous single-dish observations. Using a fitting tool developed at the Nordic ALMA Regional Center at Onsala Space Observatory (UVMULTIFIT; Martí-Vidal *et al.* 2014), initial tests to investigate the emission distributions have been performed. Although the majority of the sources are well-fitted by a Gaussian emission distribution, a significant fraction (∼20%) cannot be fitted, meaning that they exhibit a more complex circumstellar morphology. Furthermore, for some sources that show Gaussian emission distributions in all channels, the peak moves significantly between the channels. Some sources also display more complicated line profiles, indicative of a more complex velocity distribution than assumed in "the standard model", and now revealed by the extremely high sensitivity achieved compared to previous single-dish observations (Fig. 4). The observations will be analysed using a more detailed setup comparing the predicted emission from radiative transfer models with the measurements in upcoming publications giving the most accurate mass-loss-rate estimates available for these nearby sources. Sources that cannot be fitted using "the standard model" will be analysed using 3D radiative transfer along the lines described above. In addition to the CO line emission, line emission from an additional ∼20 molecular species have been detected across the two Bands (6 and 7) observed. These data will be made available to the community on the DEATHSTAR webpages (see footnote) and can be used for legacy projects.

† `www.astro.uu.se/deathstar/`

https://doi.org/10.1017/S174392131800724X Published online by Cambridge University Press

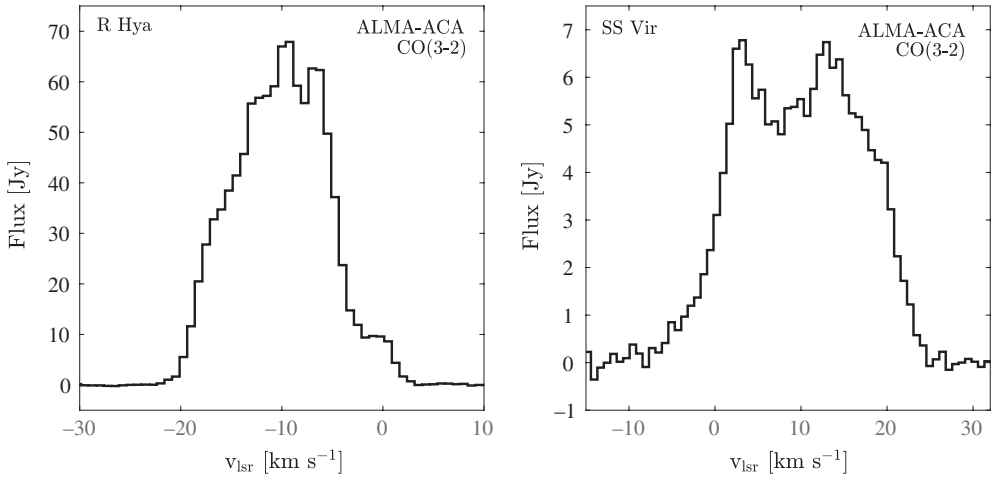

Figure 4. ALMA-ACA CO($J = 3 - 2$) line profiles for two DEATHSTAR sources (one M-type, left; one C-type, right) showing indications of a more complex velocity structure than described in "the standard model". The names are given in the upper left corner of each panel. The emission distributions of both sources can be fitted with a Gaussian in each channel.

References

Aringer *et al.* 2009, *A&A*, 503, 913
Bladh *et al.* 2015, *A&A*, 575, 105
Boyer *et al.* 2012, *ApJ*, 748, 40
Brinch & Hogerheijde 2010, *A&A*, 523, 25
Bujarrabal *et al.* 2018, *A&A*, 616, L3
Castro-Carrizo *et al.* 2010, *A&A*, 523, 59
Chiu *et al.* 2006, *ApJ*, 645, 605
Cummings *et al.* 2016, *ApJ*, 818, 84
Danilovich *et al.* 2015a, *A&A*, 574, 23
Danilovich *et al.* 2015b, *A&A*, 581, 60
De Beck *et al.* 2010, *A&A*, 523, 18
Doan *et al.* 2017, *A&A*, 605, 28
Eriksson *et al.* 2014, *A&A*, 566, 95
Goldreich & Scoville 1976, *ApJ*, 205, 384
González-Delgado *et al.* 2003, *A&A*, 411, 123
Groenewegen 2006, *A&A*, 448, 181
Groenewegen *et al.* 2007, *MNRAS*, 376, 313
Groenewegen *et al.* 2009, *A&A*, 506, 1277
Groenewegen *et al.* 2011, *A&A*, 526, 162
Groenewegen *et al.* 2016, *A&A*, 596, 50
Groenewegen 2017, *A&A*, 606, 67
Groenewegen & Sloan 2018, *A&A*, 609, 114
Guélin *et al.* 2018, *A&A*, 610, 4
Gullieuszik *et al.* 2012, *A&A*, 609, 114
Gustafsson *et al.* 2008, *A&A*, 486, 951
Hankins *et al.* 2018, *ApJ*, 852, 27
Höfner & Olofsson 2018, *A&ARv*, 26, 1
Ishihara *et al.* 2011, *A&A*, 534, 79
Ivezic *et al.* 1999, *astro-ph:* /9910475
Jones & Boffin 2017, *Nat. Astronomy*, 1, id. 0117
Justtanont *et al.* 2012, *A&A*, 537, 144

https://doi.org/10.1017/S174392131800724X Published online by Cambridge University Press

Kim *et al.* 2017, *Nat. Astronomy*, 1, id. 0060
Li *et al.* 2014, *A&A*, 568, 111
Li *et al.* 2016, *A&A*, 588, 4
Lian *et al.* 2014, *A&A*, 564, 84
Liljegren *et al.* 2017, *A&A*, 606, 6
Maercker *et al.* 2012, *Nature*, 490, 232
Maoz *et al.* 2014, *ARA&A*, 52, 107
Mamon *et al.* 1988, *ApJ*, 328, 797
Martí-Vidal *et al.* 2014, *A&A*, 563, 136
Matsuura *et al.* 2013, *MNRAS*, 429, 2527
Meixner *et al.* 2006, *AJ*, 132, 2268
Mohamed & Podsiadlowski 2012, *BaltA*, 21, 88
Nanni *et al.* 2018, *MNRAS*, 473, 5492
Ramstedt *et al.* 2006, *A&A*, 454, L103
Ramstedt *et al.* 2008, *A&A*, 487, 645
Ramstedt *et al.* 2009, *A&A*, 499, 515
Ramstedt *et al.* 2011, *A&A*, 531, 148
Ramstedt *et al.* 2014, *A&A*, 570, L14
Ramstedt *et al.* 2017, *A&A*, 605, 126
Ramstedt *et al.* 2018, *A&A*, 616, 61
Riebel *et al.* 2012, *ApJ*, 753, 71
Sahai 1992, *A&A*, 253, L33
Sargent *et al.* 2011, *ApJ*, 728, 93
Schöier & Olofsson 2001, *A&A*, 368, 969
Schöier *et al.* 2005, *A&A*, 432, 369
Srinivasan *et al.* 2006, *AAS*, 38, 1121
Teyssier *et al.* 2006, *A&A*, 450, 167
van Loon *et al.* 2005, *A&A*, 438, 273
Vlemmings *et al.* 2018, *A&A*, 613, L4

Discussion

Whitelock: Fascinating that you choose R For as the example showing uniform mass loss. Near IR-photometry (Feast *et al.* 1984, MNRAS 211, 331) shows very non-uniform dust mass-loss rate.

Ramstedt: Indeed it is not the case for a lot of the sources where we know of asymmetries from probes of different (smaller) scales that we see any signs of this on the large (100s of AU) scales probed by the CO line profiles.

Sahai: In heating-cooling models of CO emission from CSEs (e.g. Sahai 1990), CO/H_2 and dust properties are coupled-in, so with good enough data, one can constrain these as well. ALMA observations (e.g. with DEATHSTAR) is now hopefully going to provide such data!

Ramstedt: Yes, indeed, increasing the number of lines, also from other molecules than CO, allows for a better constrained model of the CSE.